Crystal Structure of Heme Oxygenase from the Gram-Negative Pathogen *Neisseria meningitidis* and a Comparison with Mammalian Heme Oxygenase-1†

David J. Schuller,‡,§ Wenming Zhu,|| Igor Stojiljkovic,|| Angela Wilks,⊥ and Thomas L. Poulos*,‡

Department of Molecular Biology & Biochemistry, Department of Physiology & Biophysics, and Program in Structural Biology, University of California, Irvine, California 92697-3900, Department of Microbiology & Immunology, Emory University School of Medicine, Atlanta, Georgia 30322, and Department of Pharmaceutical Sciences, School of Pharmacy, University of Maryland, Baltimore, Maryland 21201

Received May 18, 2001

ABSTRACT: We report the crystal structure of heme oxygenase from the pathogenic bacterium *Neisseria meningitidis* at 1.5 Å and compare and contrast it with known structures of heme oxygenase-1 from mammalian sources. Both the bacterial and mammalian enzymes share the same overall fold, with a histidine contributing a ligand to the proximal side of the heme iron and a kinked α-helix defining the distal pocket. The distal helix differs noticeably in both sequence and conformation, and the distal pocket of the *Neisseria* enzyme is substantially smaller than in the mammalian enzyme. Key glycine residues provide the flexibility for the helical kink, allow close contact of the helix backbone with the heme, and may interact directly with heme ligands.

Heme oxygenase (HO)[1] catalyzes the conversion of heme to biliverdin in a multistep reaction (Figure 1) (*1*). The reaction requires three oxygen molecules and a number of reducing equivalents, and reaction products include iron and CO. For the human enzymes, cytochrome P450 reductase provides the reducing equivalents. The HO reaction is essential for the recycling of iron from heme, but also serves a variety of specific needs in different branches of life. In vertebrates, the HO reaction is important for heme homeostasis and oxidative stress response. The location of one HO isozyme (HO-2) in neural tissue has also raised the possibility that HO-generated carbon monoxide may be a messenger (*2*). In photosynthetic organisms including cyanobacteria, algae, and higher plants, biliverdin is used as a starting point for the construction of linear tetrapyrrole pigments for photosynthesis or light-sensing (*3*). In pathogenic bacteria, HO is part of a pathway for mining iron from host heme (*4, 5*).

Most biochemical, kinetic, and spectroscopic studies of HO have been carried out with the HO-1 isozyme from rats and humans recombinantly expressed in *E. coli*. Key findings include identification of the proximal histidine heme iron ligand, identification of the reaction intermediates hydroxyheme and verdoheme, and measurement of association and dissociation rates for oxygen and CO ligands (*6*−*8*). These studies underscore the several unusual features of the HO reaction. For example, the heme serves as both substrate and cofactor, the reaction is regiospecific for the α-*meso* edge of the heme, and HO is more resistant to carbon monoxide (CO) poisoning than the globins (*6*). In addition, unlike peroxidases and P450s, HO does not utilize an oxyferryl (Fe^{4+}═O) intermediate as the active hydroxylating species but instead utilizes an electrophilic peroxy intermediate (*7, 9, 10*).

Recently, HO has been identified in the Gram-positive bacterium *Corynebacterium diphtheriae* (*5, 11*) and the Gram-negative bacterium *Neisseria* meningitidis (*4, 12*). The *C. diphtheriae* enzyme shares nearly 35% of its sequence with the core of human HO-1, with the strongest conservation showing up in the distal helix (*5*). The sequence of HO from *N. meningitidis* has less than 25% identity with that of human HO-1, and is substantially different even in the distal helix, the most highly conserved region in all previously characterized forms of the enzyme (*4*). The reaction catalyzed by *N. meningitidis* HO appears to be the same as for HO-1, including its regioselectivity (*12*). One difference already noted is that the reaction product is ferric biliverdin IXα rather than reduced iron and free biliverdin IXα (*4*). This difference in product may be the result of assaying the reaction with NADPH cytochrome P450 reductase rather than the native bacterial electron donor, which is still unknown. Both enzymes produce ferric biliverdin when the reductase system is replaced with ascorbate.

Recently we solved the crystal structure of human HO-1 (*13*), which was followed by solution of the rat HO-1 structure (*14*). These structures revealed the surprising lack of a basic side chain in the distal pocket that could serve as

† D.J.S. and T.L.P. were funded by NIH Grant GM33688. A.W. was funded by NSF POWRE Grant 0074609. W.Z. and I.S. were funded by NIH Grants AI45883 and AI42870. This work is based upon research conducted at the Stanford Synchrotron Radiation Laboratory (SSRL), which is funded by the Department of Energy (BES, BER) and the National Institutes of Health (NCRR, NIGMS).

* Corresponding author. E-mail: poulos@uci.edu.

‡ University of California, Irvine.

§ Current address: Department of Molecular Biology & Genetics, 209 Biotechnology Building, Cornell University, Ithaca, NY 14853.

|| Emory University School of Medicine.

⊥ University of Maryland.

[1] Abbreviations: HO, heme oxygenase; HO-1, mammalian HO isozyme 1; CO, carbon monoxide; MAD, multiple wavelength anomalous diffraction; heme, Fe-protoporphyrin IX.

10.1021/bi0110239 CCC: $20.00
Published on Web 08/23/2001

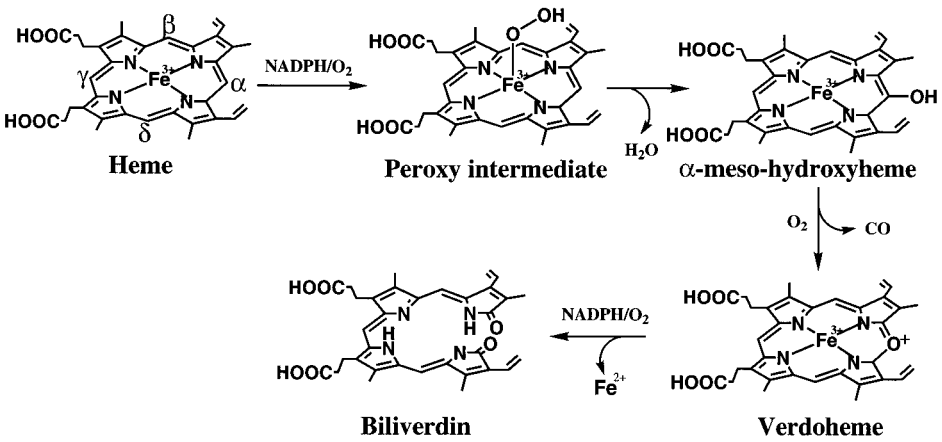

FIGURE 1: Catalytic cycle of heme oxygenase.

an acid/base catalyst or source of protons as found in peroxidases (*13*). Crystallization has also been reported for HO from the Gram-positive pathogenic bacterium *Corynebacterium diphtheriae* (*15*).

We report here the crystallization of HO from *N. meningitidis* and describe its three-dimensional structure. The low sequence similarity between this protein and mammalian HO-1, especially in the active site, provides further insight into which features of the enzyme may be important in the enzymatic reaction.

MATERIALS AND METHODS

Crystallization. Neisseria meningitidis HO was purified from a recombinant *E. coli* system and reconstituted with heme as previously described (*12*). Crystallization conditions were discovered through use of the CrystalScreen kit, condition 22 (Hampton Research, Laguna Niguel). Optimized conditions for crystallization consisted of vapor diffusion with the reservoir containing 0.1 M Tris-HCl, pH 8.5, 0.2 M sodium acetate, and 32.5% poly(ethylene glycol) 3350, and sitting drops consisting of 5 μL of reservoir and 5 μL of protein stock at 32 mg/mL. Crystals grew in approximately 1 week. The naturally cryoprotective nature of the mother liquor simplified low-temperature data collection. The crystals belong to the tetragonal space group $P4_32_12$ with cell dimensions $a = b = 63.167$ Å, $c = 100.378$ Å with one molecule per asymmetric unit.

Data Collection and Processing. Crystals were frozen in a nitrogen stream, and data were collected at 120 K. MAD data were collected from a single crystal at four wavelengths on SSRL beamline 1−5. At each wavelength, 2 scans of 30 frames were collected with a phi rotation of 2° per frame. Scans and wavelengths were cycled in five frame wedges. High-resolution data were collected from a different single crystal at SSRL beamline 9−1 in separate high- and low-resolution scans. Data were integrated and scaled with DENZO and SCALEPACK (*16*). Data statistics are summarized in Table 1. Additional data processing was carried out with the CCP4 suite (*17*).

Phasing. The iron peak was clearly visible in anomalous difference Patterson maps, and the site was located with HEAVY (*18*). The iron position was refined and MAD phases calculated using SHARP (*19*) followed by density modification in SOLOMON (*20*), which produced maps suitable for model fitting.

Table 1: Data Statistics[a]

	data set				
	MAD1	MAD2	MAD3	MAD4	Hi-res
(Å)	1.5498	1.7377	1.7401	1.9075	0.78
resolution (Å)	2.0	2.20	2.20	2.45	1.50
I/σ	57.2	53.7	53.3	45.4	13.3
% completeness	71.1	70.8	70.9	70.9	94.9(92.1)
no. of observations	71469	52669	53538	38661	161249
no. of reflections	10310	7770	7777	5700	31367
linear R	0.048	0.044	0.043	0.045	0.047(0.532)
mosaicity (deg)	0.846	0.838	0.835	0.858	1.143
PhP, centric, isomorphous	−	4.9	3.1	0.59	
PhP, acentric, isomorphous	−	4.8	4.6	0.63	
PhP, acentric, anomalous	2.6	3.2	2.6	0.63	

[a] Values in parentheses are for the outermost shell, 1.53−1.50 Å, for the Hi-res data. Data processing and scaling numbers are as reported by DENZO and SCALEPACK (*16*). The linear R-factor is $\Sigma(|(I - \langle I \rangle)|)/\Sigma(I)$, where single measurements are excluded. PhP = phasing power, as reported by SHARP (*19*).

Table 2: Model Statistics[a]

resolution	44−1.50 Å
Ramachandran angles	
most favored	94.4%
additional allowed	5.6%
R	22.7%
R-free	26.2%
FOM	0.786
RMS(bond)	0.017
RMS(angle)	1.543
RMS(chiral)	0.099
protein atoms (excluding H)	1576
heme atoms	43
solvent atoms	244

[a] R values and geometry statistics are reported by REFMAC5 (*24*).

Model Building and Refinement. Initial model building was performed with the Alberta/CalTech version of TOM (M. Israel and A. Chirino, personal communication), a version of FRODO (*21*). The sequence was obtained from GenBank entry AF133695 (*22*) and adjusted to reflect the fact that translation begins at the second rather than the first Met. Later rounds of modeling requiring alternate conformations were carried out using XtalView Xfit (*23*). REFMAC (*24*) with a maximum-likelihood target was used for refinement. The last few rounds of refinement were carried out with

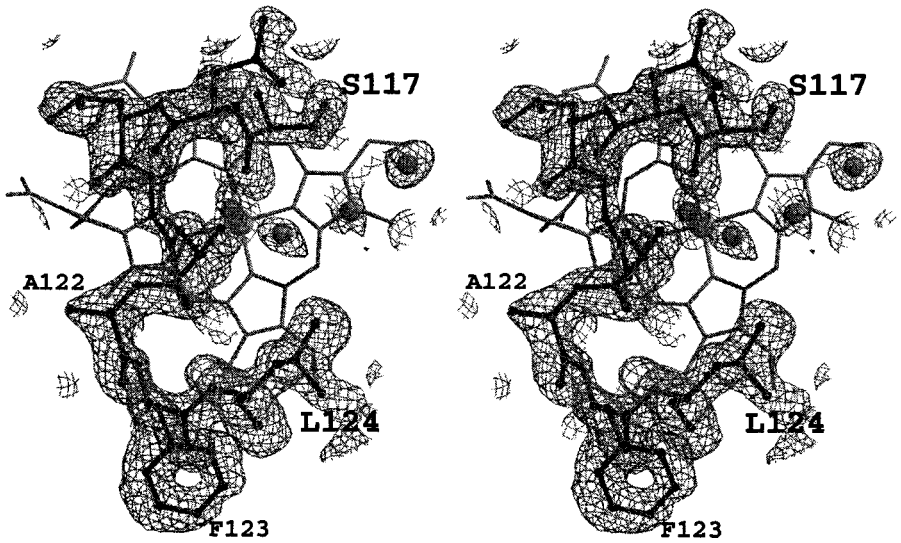

FIGURE 2: Stereo diagram of the $2F_o-F_c$ composite-omit electron density map contoured at 1σ showing part of the distal helix.

anisotropic thermal factors. Coordinates have been deposited in the Protein Data Bank under accession number 1J77.

Structure Analysis. Cavity volumes were calculated with VOIDOO (*25*). The numbers reported are probe-accessible volumes for a 1.4 Å radius sphere with heme and polypeptide excluded. A composite omit map was constructed using CNS (*26*). Data from 45 to 1.5 Å were included, and each calculation omitted 3% of the molecule. A section of the composite-omit electron density map for the distal helix is shown in Figure 2. Analysis with PARVATI revealed no nonpositive definites, no atoms with anisotropy less than 0.2, and no atoms with perfect isotropy (*27*). Mean thermal anisotropy for all atoms was 0.85 with a sigma of 0.093.

RESULTS

Overall Structure. A superposition of the folds of human HO-1 and *N. meningitidis* HO is shown in Figure 3. The two enzymes obviously share a homologous, largely α-helical fold, despite the low sequence identity. The overall RMS deviation for 146 common Cα atoms is 1.73 Å (*28*). In the *N. meningitidis* enzyme, the C terminus wraps around toward the front of the molecule (as depicted in Figure 3) where the heme binding pocket is located. The location of the corresponding C-terminal region in HO-1 is undoubtedly quite different since the C-terminal tail is used to anchor HO-1 to the microsomal membrane. This region was eliminated from HO-1 for the structural work (*13*). The bacterial HO is more compact, with shortened surface loops (e.g., residues 89−92 and 132−138) and with one helix replaced by an extended chain (residues 96−104 replace HO1:109−126).

Proximal (His Ligand) Side. A comparison between the two structures in the region surrounding the His heme ligand is shown in Figure 4. As expected from the sequence alignments, the structures are very similar in this region. His-23 contributes the proximal heme ligand, taking the place of HO-1:His-25. In both enzymes, a neighboring carboxylate can accept an H-bond from the His ligand. In HO-1, Glu-29 serves this purpose, but the comparable residue in the *N. meningitidis* enzyme, Asp-27, is not in position for H-bonding. Instead, Asp-24, which is Thr-26 in HO-1 and Ile-26 in rat HO-1, is in position to H-bond with the N atom of the His ligand. Since the His−carboxylate pairs are solvent-exposed, these H-bonding interactions are probably weak. This is consistent with resonance Raman studies, which indicate that the proximal His residue is not strongly hydrogen-bonded (*29, 30*).

The packing of side chains on the proximal face of the heme is very similar in the two enzymes. Thr19 contacts the proximal side of the heme through a water molecule, in the same manner as HO-1:Thr-21. Phe-181 under the *β-meso* edge and Tyr-112 near the 6-propionate fill almost exactly the same positions as HO-1:Phe-207 and HO-1:Tyr-134. Val26 under the α-*meso* edge replaces HO-1:Ala-28. As previously mentioned, the C-terminus curls back toward the active site so that Pro206 is less than 4 Å from Asp24 and Asp27. The final three residues of the sequence, His-Arg-His, are not ordered in the electron density map.

Heme Orientation and Propionate Interactions. NMR studies of HO-1 indicated that the heme may be in two orientations, flipped 180° about the $\alpha-\gamma$ axis (*31*). In fact, the electron density for methyl and vinyl groups in the HO-1 crystal structure was weak (*13*). The heme in the current structure was placed in the same orientation as in HO-1, but the density for methyl and vinyl groups is much more solid, indicating that the bacterial enzyme may not undergo the same degree of heme-flipping. The 7-propionate, which is solvent-exposed, is somewhat disordered and is modeled as two alternate conformations.

HO-1 contains a number of ionic/H-bonding interactions between the heme propionates and nearby side chains which appeared to be important for orienting the heme in the active site. Somewhat surprisingly, these interactions are not well conserved in *N. meningitidis* HO. Lys16 and Tyr112 of the *N. meningitidis* enzyme correspond to HO-1:Lys-18 and HO-1:Tyr-134, respectively. However, there are no basic side chains in the *N. meningitidis* enzyme corresponding to HO-1:Arg183 and HO-1:Lys179 (Figure 4). Instead, Trp-153 fills the space taken by HO-1:Arg183 and HO-1:Lys-179. The relative importance of HO-1:Arg-183 has been examined by site-directed mutagenesis. Replacement of Arg-183 with Glu or Asp, but not with other residues including Gln and Asn, reportedly led to significant detectable changes in regio-selectivity (*32*). The lack of conservation of this interaction

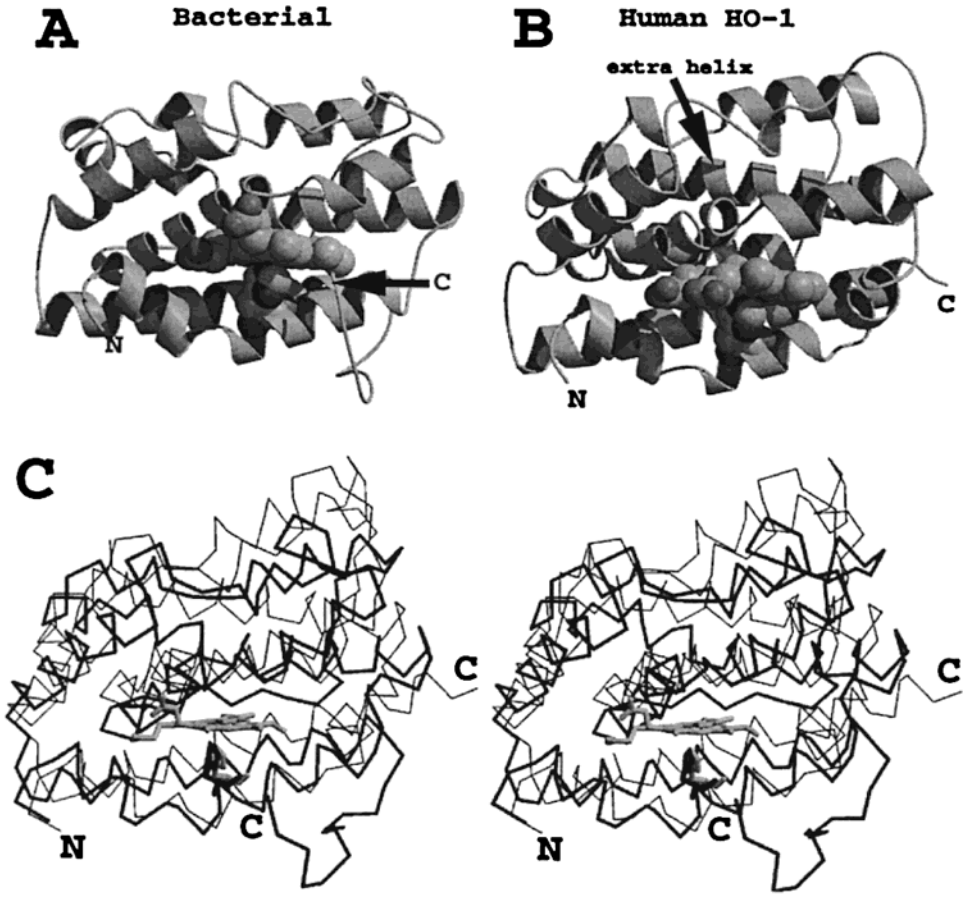

FIGURE 3: Comparisons of human HO-1 and *N. meningitidis* HO. Panels A and B are models of *N. meningitidis* HO and human HO-1, respectively. Both the heme and proximal His ligand are shown. Panel C is a stereo diagram showing the least-squares superimposition of both structures with *N. meningitidis* HO represented by the thicker lines.

in the *Neisseria* enzyme raises questions about its general importance.

Distal Helix. An important feature we noted in HO-1 is the distortion in the helix that covers part of the heme distal surface as well as forming part of the O_2 binding pocket (*13*). The distal helix of *N. meningitidis* HO also is distorted, but there are important differences when compared to HO-1 (Figure 5). In HO-1, the two molecules in the crystal asymmetric unit had different conformations in their distal helices, with one characterized as more 'open' and the other as more 'closed' (*13*). The distal helix in *N. meningitidis* HO is clearly in a 'closed' conformation, and is closer to the heme iron and water ligand than in HO-1. This means that the water ligand is more deeply enmeshed in the distal helix, within contact distance (3.14−3.61 Å) of backbone atoms from Gly-116, Ser-117 and Gly-120.

The differences in the distal helix between the mammalian and bacterial enzymes go beyond what can be explained by the capture of different transient states in the crystal lattice. In *N. meningitidis* HO-1, 12 residues in the distal helix, Cys-113−Le-124, cover nearly the same distance as 13 residues, Thr-135−Leu-147, in HO-1. The helix of the bacterial enzyme is more severely kinked to allow this disparity. The sequence identity in this stretch is remarkably low. Throughout this stretch, only three residues in the distal helix are approximately structurally conserved between the two HO structures. Leu-124 over the heme 2-vinyl group approximately fills the place of HO-1:Leu147 although the superposition is not exact. Gly120 over the D-pyrrole ring takes the place of HO-1:Gly-143, and Gly-116 approximately takes the place of HO-1:Gly139 although the Cα of Gly-116 points out toward the propionates rather than straight down toward the heme plane. This places the peptide bond between Gly116 and Ser117 toward the heme. As for Leu119, it does not take the place of HO-1:Leu141. Instead of pointing up away from the heme, its side chain angles down to contact the *γ-meso* heme edge such that it occupies the space taken byHO-1:Ser142 (Figure 5). The closest polar side chains to the distal face of the heme are gone: Ala117 replaces HO-1:Arg136 while HO-1:Asp140 falls between the positions of Ser117 and Asn-118. Asn118 points up away from the heme while the Ser117 side chain approximately fills the position of a water which was hydrogen-bonded to the HO-1:Asp-140 side chain. The alcohol group of Ser-117 forms hydrogen bonds with the peptide backbone, which helps to stabilize the distal helix distortion. Finally, HO-1:Gly144 is replaced by Ala-121.

Distal Pocket. As in HO-1, continuous electron density between the heme iron and the distal side coordination position at a distance of ≈2.0 Å indicates that water is coordinated to the heme iron, which is consistent with spectroscopic results (*12*) (Figure 5). Both structures have a polar, hydrophilic pocket over the distal side of the heme, The nature of the distal pocket is similar in the two HO structures, but there are very few conserved amino acid residues. For example, the α-*meso* heme edge still contacts a hydrophobic wall, but all of the specific residues involved are changed: HO-1:Met34, Phe214, and Asn210 are replaced

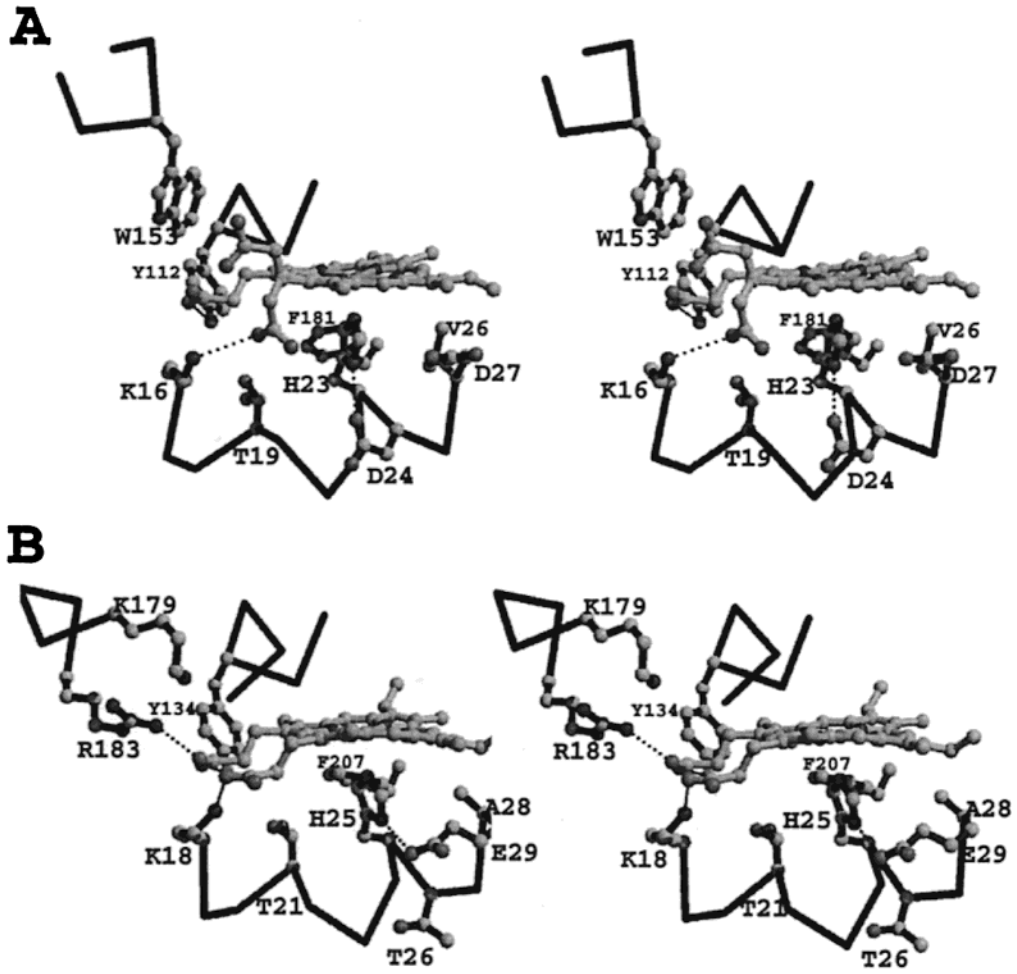

FIGURE 4: Stereo diagram comparing the proximal heme region in (A) *N. meningitidis* and (B) human HO-1. Note the two alternate conformations of the heme 7-propionate in *N. meningitidis* HO. Heteroatoms within 3.5 Å distance from one another are indicated by a dashed line. Lys18 in HO-1 and Lys16 in *N. meningitidis* HO are 3.5 and 3.35 Å, respectively, from a heme propionate, indicating rather weak H-bonding interactions. In HO-1, Arg183 is ≈2.9 Å from the heme propionate, indicating a stronger H-bonding/ionic interaction although this interaction is not conserved in *N. meningitidis* HO.

by Val30, Leu188, and Tyr184. His-141 and His-53 fill the space of HO-1:Phe166 and HO-1:Tyr-58 at the top of the pocket (not shown in Figure 5). The distal pocket is smaller in *N. meningitidis* HO. The smaller pocket in the bacterial HO is reflected by the solvent-accessible volume of the pocket, which is 7.5 $Å^3$, while the corresponding volumes for the two known mammalian HO-1 structures run from 43.6 to 59.7 $Å^3$ (*13*, *14*). The polar, hydrophilic nature of the distal pocket is illustrated by the appearance of several ordered solvent molecules in the electron density map (Figures 2 and 5). The *N. meningitidis* enzyme seems to lack the "hydrophobic inner chamber" noted in the mammalian enzyme, and this accounts for much of the volume difference (*13*).

DISCUSSION

N. meningitidis HO is phylogenetically quite distant from HO-1, and the sequences share less than 25% identity (*4*, *22*). The difference in sequences extends even into the distal helix, which is well conserved in all previously characterized forms of HO. The current structure provides an excellent opportunity to examine two distantly related HOs and try and extract those structural features critical for catalysis. The availability of human and pathogen structures also opens up the possibility for the design of specific inhibitors for medicinal purposes.

In previous structures of mammalian HO, a large segment preceding the C-terminal membrane anchor was either missing (*13*) or not resolved (*14*). The correspondence of the fold of *N. meningitidis* HO to that of mammalian HO reinforces earlier claims that the missing segment of the mammalian proteins is not vital for catalysis (*33*, *34*). The structure and purpose, if any, of the extra segment in mammalian HO remain unknown.

There are many differences between the *N. meningitidis* HO and the mammalian HO-1 structures, and yet the two versions of the enzyme catalyze the same reaction with the same regioselectivity. If we assume that the mechanism is also the same, then we should ask which structural features are retained and which are not, especially near the active site. The proximal His ligand and the general layout of other proximal residues are conserved. On the distal side of the heme, the differences are manifold. No acidic or basic side chains are conserved, which eliminates the possibility of a direct conserved role in the reaction for any distal protein side chains. However, Gly-116 and Gly-120 are conserved in all HOs for which sequence and functional information is available indicating that kinking and flexibility of the distal

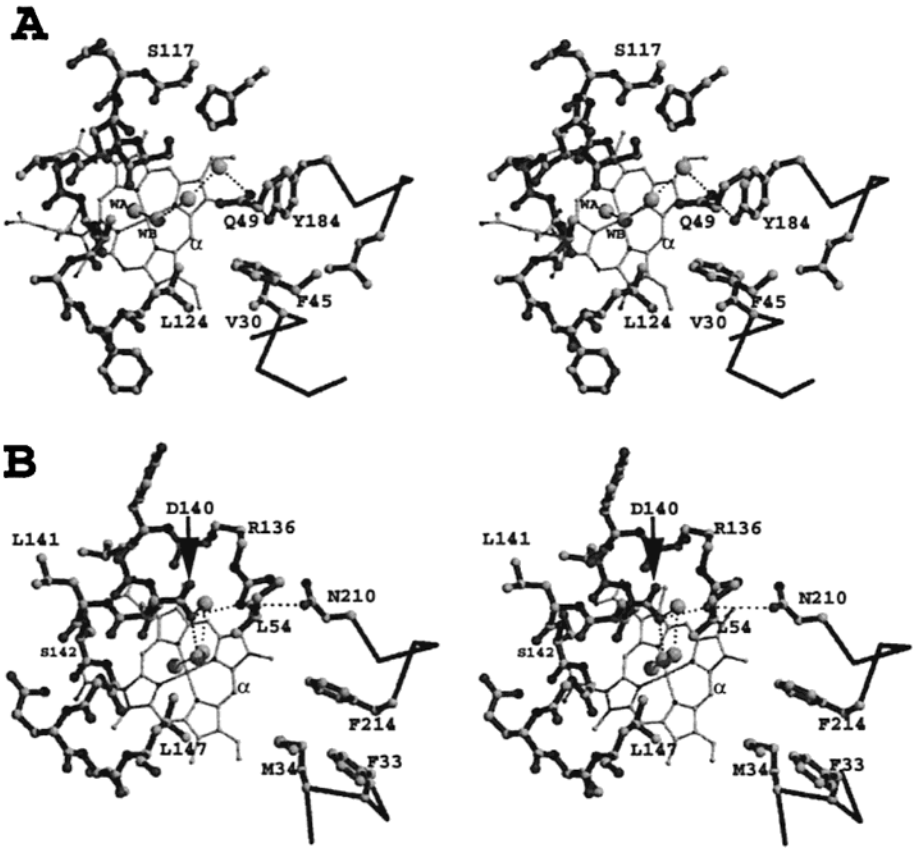

FIGURE 5: Stereo diagrams showing the distal pocket in (A) *N. meningitidis* HO and (B) human HO-1. As in Figure 4, heteroatoms within 3.5 Å of other atoms are denoted by dashed lines. In panel A, the water coordinated to the heme iron is labeled WA, and the water contacting both WA and the α-*meso* heme carbon is labeled WB. WA in panel A is the axial water ligand while WB forms a 2.9 Å H-bond with WA. WB also is ≈3.4 Å from the α-*meso* heme carbon.

helix is a critical element in HO function. Although the *N. meningitidis* enzyme retains the distinct kink and key glycines responsible for the helical distortion found in HO-1, the detailed position of the distal helix and the orientation of specific residues differ considerably. This may have more to do with the inherent flexibility of the distal helix as opposed to important functional differences between HOs. The distal helices in both molecules in the asymmetric unit of human HO-1 were positioned differently with respect to the heme and exhibited high thermal factors (*13*), clearly indicating that the distal helix is quite mobile. The conformation of the distal helix in the rat HO-1 structure also differed from that of human HO-1 (*14*), and a recent NMR study of human HO-1 confirms that parts of the distal helix are probably mobile (*31*). It may well be that in the *N. meningitidis* HO structure the distal helix was captured in one of several energetically accessible conformational states.

The close approach of the distal helix to the distal Fe water ligand reinforces our earlier conclusion that the steric influence of the distal helix is primarily responsible for the regioselectivity of the reaction, both by protecting the other three *meso* edges of the heme and by directing the oxygen ligand toward the α-*meso* edge. This is in agreement with the recent NMR work which also found a closer approach of the distal helix in human HO-1 than in the crystal structure (*31*). The close approach of the distal helix raises the possibility that interactions with the oxygen complex may be as much with the first oxygen atom as with the second. The ordered solvent structure in the active site may be illustrative of the steric control. Note that water ligand WA in Figure 5 is 3.0 Å from water WB for a possible H-bond while water WB is 3.4 Å from the α-*meso* heme carbon. This could foreshadow how O_2/peroxide is oriented in the distal pocket, thus directing the peroxide toward the α-*meso* carbon for regioselective hydroxylation.

It appears that the only protein groups that would interact directly with a peroxy ligand are in the distal helix peptide backbone, and since there are no catalytic side chains involved, a good deal of sequence variation can be tolerated. Asp-140 (*35*), Gly-139, and Gly-143 (*36*) in human HO-1 have all been targeted for mutagenesis. A consistent finding is that in most of the mutants, HO-1 now forms a species with spectral properties of a peroxidase-like Compound I ferryl intermediate and the mutants exhibit peroxidase activity. The peroxidase activity is a consequence of forming the ferryl species, which readily reacts with traditional phenolic peroxidase substrates. The relationship between the loss of HO activity and the gain in peroxidase activity (*36*) further underscores that HO operates by electrophilic addition of a peroxide O atom to the heme and not via a ferryl intermediate. It thus appears that HO is designed to stabilize the peroxy complex long enough for the electrophilic addition mechanism to dominate (P. R. Ortiz de Montellano, personal communication). In the absence of direct structural data on the HO-1 mutants, the most straightforward explanation for their behavior is that substitution at these sites alters the conformation of the distal helix and therefore its interaction with ligands.

Both the bacterial and mammalian enzymes have a polar, hydrophilic pocket over the α-*meso* heme edge, which must

be necessary to accommodate the various intermediates and ligands. The reaction is known to proceed through hydroxyheme and verdoheme on the way to the biliverdin product, with three distinct oxygenation steps and the release of CO. The pocket is much smaller in *N. meningitidis* HO than in HO-1, mostly due to the absence of the hydrophobic inner cavity noted for the human structure (*13*). It seems unlikely that the *Neisseria* enzyme could utilize heme analogues modified with bulky groups at the 1−4 positions, as the human enzyme can (*37*). It might also be interesting to investigate whether it differs in the kinetics of CO extrusion.

One final similarity to be noted is the asymmetric distribution of polar and nonpolar residues over the heme shared by both *N. meningitidis* HO and HO-1. On the proximal side, a polar residue sits under the A ring (Asp-27) while a nonpolar residue sits under the B ring (Phe-181). On the distal side of the heme, this is reversed: a nonpolar residue (Leu-124) is near the A ring while a spacious polar pocket opens up atop the B ring. This may be of some relevance, especially considering that the HO reaction consists of three consecutive oxygenation steps. The similar pattern of polar vs nonpolar residues on both sides of the heme in both HOs prompts us to propose that the reaction intermediates will pucker in the same direction in both enzymes. Further insight into this hypothesis will undoubtedly require structural data of the various intermediates.

To summarize, the proximal side of the heme looks very similar in the current structure and existing mammalian HO-1 structures, while on the distal side only a few commonalities are observed, including these key features: (a) the distal helix makes a close approach to the heme so that contacts are with helical backbone atoms, and (b) a kink in the distal helix right over the heme opens up a loop of the helix for interactions with ligands and allows for flexibility. Conserved glycine residues (nearly the only distal residues conserved) allow for both of these features.

ACKNOWLEDGMENT

We thank Henry Bellamy for help with data collection on SSRL MAD beamline 1−5, Evan Bursey for assistance with data collection and transportation, and Huiying Li, J. P. Cartailler, and William N. Lanzilotta for helpful discussions.

REFERENCES

1. Tenhunen, R., Marver, H. S., and Schmid, R. (1969) *J. Biol. Chem. 244*, 6388−6394.
2. Maines, M. D. (1997) *Annu. Rev. Pharmacol. Toxicol. 37*, 517−554.
3. Beale, S. I. (1994) in *The molecular biology of cyanobacteria* (Bryant, D. A., Ed.) pp 519−558, Academic Publishers, Dordrecht, The Netherlands.
4. Zhu, W., Hunt, D. J., Richardson, A. R., and Stojiljkovic, I. (2000) *J. Bacteriol. 182*, 439−447.
5. Schmitt, M. P. (1997) *J. Bacteriol. 179*, 838−845.
6. Migita, C. T., Matera, K. M., Ikeda-Saito, M., Olson, J. S., Fujii, H., Yoshimura, T., Zhou, H., and Yoshida, T. (1998) *J. Biol. Chem. 273*, 945−949.
7. Ortiz de Montellano, P. R. (1998) *Acc. Chem. Res. 31*, 543−549.
8. Ortiz de Montellano, P. R. (2000) *Curr. Opin. Chem. Biol. 4*, 221−227.
9. Wilks, A., and Ortiz de Montellano, P. R. (1993) *J. Biol. Chem. 268*, 22357−22362.
10. Davydov, R. M., Yoshida, T., Ikeda-Saito, M., and Hoffman, B. M. (1999) *J. Am. Chem. Soc. 121*, 10656−10657.
11. Wilks, A., and Schmitt, M. P. (1998) *J. Biol. Chem. 273*, 837−841.
12. Zhu, W., Wilks, A., and Stojiljkovic, I. (2000) *J. Bacteriol. 182*, 6783−6790.
13. Schuller, D. J., Wilks, A., Ortiz de Montellano, P. R., and Poulos, T. L. (1999) *Nat. Struct. Biol. 6*, 860−867.
14. Sugishima, M., Omata, Y., Kakuta, Y., Sakamoto, H., Noguchi, M., and Fukuyama, K. (2000) *FEBS Lett. 471*, 61−66.
15. Chu, G. C., Park, S.-Y., Shiro, Y., Yoshida, T., and Ikeda-Saito, M. (1999) *J. Struct. Biol. 126*, 171−174.
16. Otwinowski, Z., and Minor, W. (1997) *Methods Enzymol. 276*, 307−326.
17. Collaborative Computational Project (1994) *Acta Crystallogr., Sect. D D50*, 760−763.
18. Terwilliger, T. C., and Kim, S.-H. (1987) *Acta Crystallogr., Sect. A A43*, 1−5.
19. de La Fortelle, E., and Bricogne, G. (1997) *Methods Enzymol. 276*, 472−494.
20. Abrahams, J. P., and Leslie, A. W. G. (1996) *Acta Crystallogr., Sect. D D52*, 30−42.
21. Jones, T. A. (1985) *Methods Enzymol. 115*, 157−171.
22. Zhu, W., Hunt, D. J., Richardson, A. R., and Stojiljkovic, I. (2000) DDBJ/EMBL/Genbank Databases.
23. McRee, D. E. (1992) *J. Mol. Graphics 10*, 44−46.
24. Murshudov, G. N., Vagin, A. A., and Dodson, E. J. (1997) *Acta Crystallogr., Sect. D D53*, 240−255.
25. Kleywegt, G. J., and Jones, T. A. (1994) *Acta Crystallogr., Sect. D D50*, 178−185.
26. Brunger, A. T., Adams, P. D., Clore, G. M., DeLano, W. L., Gros, P., Grosse-Kunstleve, R. W., Jiang, J.-S., Kuszewski, R. F., Nilges, M., Pannu, N. S., Read, R. J., Rice, R. J., Rice, L. M., Simonson, T., and Warren, G. L. (1998) *Acta Crystallogr., Sect. D D54*, 905−921.
27. Merritt, E. A. (1999) *Acta Crystallogr., Sect. D D55*, 1109−1117.
28. Kleywegt, G. J., and Jones, T. A. (1997) *Methods Enzymol. 277*, 525−545.
29. Sun, J., Wilks, A., Ortiz de Montellano, P. R., and Loehr, T. M. (1993) *Biochemistry 32*, 14151−14157.
30. Takahashi, S., Wang, J., Rousseau, D. L., Ishikawa, K., Yoshida, T., Takeuchi, N., and Ikeda-Saito, M. (1994) *Biochemistry 33*, 5531−5538.
31. La Mar, G. N., Asokan, A., Espiritu, B., Yeh, D. C., Auclair, K., and Ortiz de Montellano, P. R. (2001) *J. Biol. Chem. 276*, 15676−15687.
32. Zhou, H., Migita, C. T., Sato, M., Sun, D. Y., Zhang, X. H., Ikeda-Saito, M., Fujii, H., and Yoshida, T. (2000) *J. Am. Chem. Soc. 122*, 8311−8312.
33. Wilks, A., Medzihradszky, K. F., and Ortiz de Montellano, P. R. (1998) *Biochemistry 37*, 2889−2896.
34. Schuller, D. J., Wilks, A., Ortiz de Montellano, P. R., and Poulos, T. L. (1998) *Protein Sci. 7*, 1836−1838.
35. Lightning, L. K., Huang, H., Moënne-Loccoz, P., Loehr, T. M., Schuller, D. J., Poulos, T. L., and Ortiz de Montellano, P. R. (2001) *J. Biol. Chem. 276*, 10612−10619.
36. Liu, Y., Lightning, L. K., Huang, H. W., Moenne-Loccoz, P., Schuller, D. J., Poulos, T. L., Loehr, T. M., and de Montellano, P. R. O. (2000) *J. Biol. Chem. 275*, 34501−34507.
37. Frydman, R. B., Tomaro, M. L., Buldain, G., Awruch, J., Diaz, L., and Frydman, B. (1981) *Biochemistry 20*, 5177−5182.

BI0110239